Investigation of a Wideband BiCMOS Fully On-Chip W-Band Bowtie Slot Antenna

Shiji Pan, Leland Gilreath, Payam Heydari, and Filippo Capolino

***Abstract*—Design and implementation of a W-band on-chip bowtie-shaped slot antenna fabricated in 180-nm BiCMOS process is presented, and its performance and limitations are discussed. This antenna has a measured impedance bandwidth ($S_{11} < -10$ dB) across the W-band frequency range and a very wide gain bandwidth, making it a candidate for wideband applications. The measured gain for this antenna is 0–1 dBi at 94 GHz. This letter also analyzes the influence of the RF probe to the on-chip antenna performance.**

***Index Terms*—Millimeter waves, on-chip antennas (OCAs), RFIC.**

I. Introduction

SILICON technology has proven to be a viable platform for transceivers at millimeter-wave (mm-wave) frequencies. For future applications of mm-wave receivers/transmitters with on-chip antennas (OCAs), such as imaging and multi-gigabit-per-second short-range wireless communications, it is strongly desirable to design efficient and compact antennas, which would lead to fully integrated systems with performance much higher than the current state of the art. References [1] and [2] provide an elaborate review of OCAs, especially on silicon substrate at mm-waves. Despite lower gain and efficiency compared to off-chip counterparts, such as antennas in a package [3], which have been developed for 60-GHz applications [2], [4], OCAs offer the least feedline interconnection losses, which is a substantial advantage for submillimeter-wave systems. However, designing a high-gain and high-efficiency OCA is very challenging for various reasons. Because of the high permittivity and low resistivity of the silicon or SiGe substrate, an on-chip antenna will lose much of its power inside the substrate. One way to shield the OCA from the silicon substrate involves placing a ground plane at the lowest metal layer (M1) so that the thin silicon dioxide layer acts as the antenna substrate, as shown in [5]. However, because of the extremely thin thickness of silicon dioxide (i.e., less than 1% of the wavelength in silicon dioxide), the radiation efficiency is highly degraded due to ohmic losses. Furthermore, when using layer M1 as a ground, the antenna bandwidth is, in general, very narrow because of an extremely thin oxide substrate. A miniature OCA may reduce system cost and complexity, but it cannot achieve a high gain. Studies of OCAs are important to assess performance limitations of this integrated antenna solution at mm-wave frequencies, and because OCAs are expected to exhibit better performance in the higher spectrums of mm-wave and submillimeter-wave regimes, due to the increased electrical distance between M1 and M6.

Manuscript received March 06, 2013; revised May 02, 2013; accepted May 15, 2013. Date of publication May 21, 2013; date of current version June 04, 2013. This work was supported in part by the Semiconductor Research Cooperation under Project Contract 2009-VJ-1962.

The authors are with the Department of Electrical Engineering and Computer Science, University of California, Irvine, Irvine, CA 92617 USA (e-mail: shijip@uci.edu; lgilreat@uci.edu; payam@uci.edu; f.capolino@uci.edu).

Color versions of one or more of the figures in this letter are available online at http://ieeexplore.ieee.org.

Digital Object Identifier 10.1109/LAWP.2013.2264538

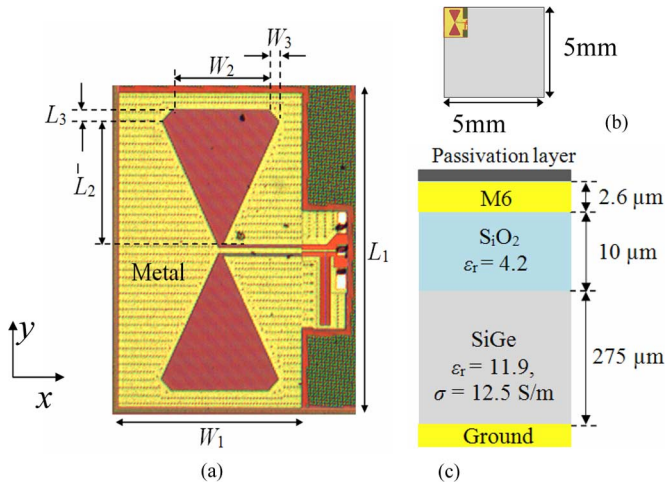

Fig. 1. (a) Micrograph of the bowtie shape slot antenna fed by a coplanar waveguide. (b) Antenna in the corner of a 5×5 mm^2 chip. (c) Side view of CMOS process used for antenna fabrication. The bowtie slot and coplanar waveguide are on metal layer six (M6).

In this letter, simulation and measurement of a W-band bowtie-shaped slot antenna fabricated in a BiCMOS process are presented. Because of the bandwidth limitations when using a ground plane on M1, we instead design and analyze the bowtie slot antenna with a ground plane below the silicon substrate. First, using full-wave simulation software, we investigate the input reflection and gain of the bowtie slot antenna as well as study the influence of a close proximity RF probe on the antenna performance. Later, we present measurements of the input reflection coefficient, radiation pattern, and gain versus frequency. As will be shown, the antenna has a very good input match ($S_{11} < -10$ dB) over the whole W-band frequency range, partly due to the severe loss in the antenna substrate. The measured gain is 0–1 dBi, which is subject to some uncertainty due to interference caused by the scattering interaction between the probe and the OCA during the measurement.

II. On-Chip Antenna Design

Fig. 1(a) shows the die micrograph of the fabricated bowtie-shaped slot antenna, whereas Fig. 1(c) illustrates the cross-sectional view of the BiCMOS process used for antenna fabrication. The bowtie slot antenna is placed on the topmost metal

layer (M6). The antenna structure is symmetrical in both x- and y-directions, except for the feeding. The antenna dimensions, indicated in Fig. 1(a), are (all in millimeters) $L_1 = 1.4$, $L_2 = 0.55$, $L_3 = 0.05$, $W_1 = 0.9$, $W_2 = 0.46$, and $W_3 = 0.05$. With the exclusion of bond pads, the core antenna occupies 1.4×0.9 mm^2 of chip area. A conductive silver adhesive layer is attached below the SiGe substrate to act as the antenna ground.

The SiGe substrate in the used technology has a thickness of 275 μm, a conductivity of 12.5 S/m, and a relative dielectric constant of 11.9. The silicon dioxide between M6 and the silicon substrate is roughly 10 μm thick with a relative dielectric constant of 4.2. Above M6, there is a passivation layer with a thickness of 0.6 μm and relative dielectric constant of 7. All the layers are included in the full-wave simulation carried out with the finite element method by HFSS. To comply with the metal density rules imposed by the foundry, arrayed 5×5-μm^2 dummy holes [small black holes as illustrated in Fig. 1(a)] are placed around the antenna metal structure on M6. Simulation results prove that the effect of these dummy holes can be ignored since each hole's size is much smaller than the guided wavelength of the substrate. A 50-Ω coplanar waveguide (CPW) is employed on M6 to feed the slot antenna and is connected to the bond pad. In the simulation, an HFSS lumped port is used to feed the CPW. The signal trace of the CPW has a 24-μm width, and the gap between the signal and each lateral ground plane is 13 μm. At W-band, the parasitic capacitance of the bond pad could slightly degrade the input matching. To solve this issue, a shunt stub is used to improve the impedance matching of bond pads to 50 Ω at the input (visible in right part of Fig. 1(a), as described in [6]). It is noteworthy that both the CPW feed and the shunt stub have negligible effect on the antenna gain and radiation pattern as observed by simulation.

The antenna is fabricated on a 5×5-mm^2 die and placed at the corner of the chip, as shown in Fig. 1(b). Due to the high dielectric constant and thickness of the SiGe substrate, surface-wave modes (TM_0 and TE_1) are excited inside the antenna substrate. It was observed from simulation that when the antenna is put at the center of the die, an increasing size of die area would result in a lower broadside gain because: 1) the peak radiation direction becomes significantly tilted away from the broadside; and 2) more surface wave losses by means of dielectric losses exist inside the lossy SiGe substrate. This makes the antenna unsuitable for broadside applications. However, when the antenna is located close to the edge of the chip, it was observed that the antenna radiation pattern and broadside gain are less susceptible to the chip size due to the edge interference and radiation at nearby chip edges, as proven by full-wave simulations.

The simulated S_{11} and broadside gain versus frequency with the antenna in the corner of a 5×5-mm^2 die as configured in Fig. 1(b) are shown in Fig. 2(c). The shunt stub is not included in the simulation. The simulated input -10-dB bandwidth covers the whole W-band frequency range, while the broadside gain at 94 GHz is around -2.5 dBi. The radiation efficiency is close to 18%, mainly due to dielectric losses and surface waves. Direct RF probing is adopted in this work to measure the antenna performance. As shown here, strong electromagnetic interference

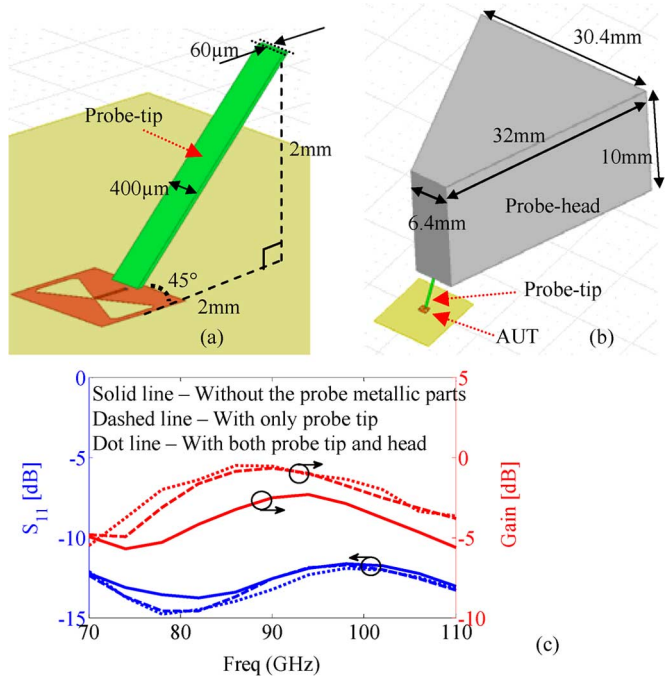

Fig. 2. (a) Three-dimensional (3-D) view of antenna and metallic probe-tip, 50 μm above the top surface of the chip. (b) 3-D view of antenna and probe-head attached to the probe tip. (c) S_{11} and broadside gain versus frequency, considering and not considering the presence of the probe. Solid line—no probe. Dashed line—with only probe tip in simulation. Dotted line—with both probe tip and probe head in simulation.

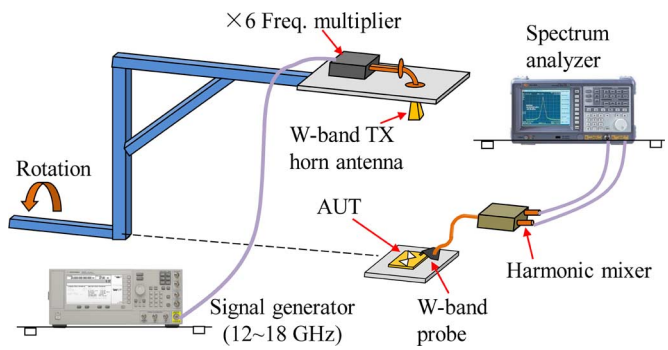

Fig. 3. Setup for the gain and radiation pattern measurement of the AUT. A calibrated horn antenna is transmitting, and the AUT is in the receiving operational mode. The AUT input reflection coefficient is instead measured by connecting a millimeter head extension directly to the probe.

is induced between probe and antenna because of their vicinity. Nevertheless, we use the probing method shown in Fig. 3 because for silicon OCA radiating broadside, it is not straightforward to realize a backside feeding scheme, as used in the measurement of in-package antennas [7], or for other mm-wave antennas as in [8]. For a backside feeding measurement scheme, even if the RF probe is in the near-field range of the antenna, the probe would have minor effect on the antenna radiation. To realize a backside feeding scheme for a silicon based OCA, an off-chip feed with the help of flip-chip or TSV technology [9] is required.

To get a reasonable estimation of the degree of performance variation caused by the probe, a probe-tip-like metallic part is included in the simulation as shown in Fig. 2(a). According to the probe datasheet (model Cascade Microtech I110-T-GSG), the

copper probe-tip is 2 mm high at a 45° inclination with respect to the chip surface. Because of the modeling difficulty here, instead of physically connecting it to the antenna, the probe-tip is "floating," and it is placed 50 μm away from the top surface of the passivation layer of the chip. Furthermore, to estimate the effect of the bulky probe-head, which is also in close range of the antenna, an additional simulation containing a copper trapezoidal structure with the probe-head dimensions was performed, as in Fig. 2(b).

Simulation plots in Fig. 2(c) compare S_{11} and gain of the antenna with and without the probe tip. Two cases are considered, as discussed above: one indicated by a dashed line where only the probe-tip is included in the simulation, and the other by a dotted line where both the probe-head and probe-tip are included. Although the simulation is based on simplifying assumptions, and without connecting the probe-tip to the antenna as in measurement, the comparison provides certain useful information on the effect the probe has on the antenna performance. It can be observed that with the probe-tip [Fig. 2(a)], the gain can be offset by 1–3 dB, and that this is mainly due to the variation of the radiation pattern. Meanwhile, S_{11} only slightly changes, mainly because it is strongly influenced by the losses in the SiGe substrate. When including the whole probe-head in the simulation [Fig. 2(b)], the radiation pattern is significantly affected as shown in Section III, especially in the E-plane, although the broadside gain is similar to the case when including only the probe-tip in the simulation. These variations are expected because the bulky probe-head is located in the antenna proximity. Therefore, during the measurements, absorbers should be used to cover the probe-head in order to partially shield its interaction with the antenna.

III. Measurement

The antenna's input reflection coefficient is measured while probing the antenna with a W-band RF probe. A short-open-load (SOL) calibration at the end of the probe-tip is conducted before the measurement. Fig. 3 illustrates the test setup for the OCA gain and radiation pattern measurements. The signal generator provides a signal in the 12–18-GHz frequency range, which is later upconverted to W-band using a $\times 6$ frequency multiplier. The W-band signal is transmitted by an off-the-shelf horn antenna with 24 dBi gain and received by the antenna under test (AUT), 30 cm away from the horn antenna. A rotation arm was built using aluminum rods and fixed in a high-resolution rotary table (not shown in Fig. 3). A metallic plate was used to hold the frequency multiplier and the transmitting (TX) horn antenna tightly on an arm. The radiation pattern of the AUT in the receiving mode is measured by rotating the arm in the E- and H-planes. The AUT output is connected to a probe that feeds an Agilent harmonic mixer and spectrum analyzer.

In the measurement, the antenna gain calibration is based on replacing the AUT with another horn antenna with known gain separated by the same distance as that between the horn and the original AUT. The horn antenna's phase center was considered as the location of the horn. Since the phase center of the horn antenna is frequency-dependent, the calibration power is adjusted based on exactly the same distance between the two phase centers. Insertion losses in the probe as well as an additional 0.5 dB transition loss between the probe and on-chip CPW were all considered in the gain calculation. Absorbers were used to cover the surface of surrounding instruments and components during the gain measurement.

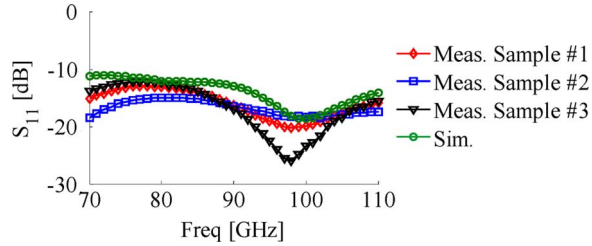

Fig. 4. Measured and simulated antenna input reflection coefficient for three different on-chip antennas.

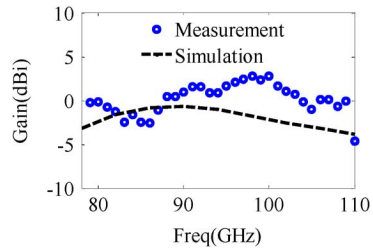

Fig. 5. Measured and simulated broadside gain of the bowtie slot antenna versus frequency.

Fig. 4 shows the comparison between the measured and simulated antenna input reflection coefficient. The simulation results are based on the simulation setup explained above where the probe tip is taken into account. To best compare to the measurement, the shunt stub is also included in the simulation. The proposed bowtie slot antenna shows a very wide -10-dB measured input return-loss bandwidth covering the entire W-band. Such a wide input impedance bandwidth is also contributed to by the significant overall losses, including surface wave, dielectric, and ohmic losses. To validate the measurements, the same test was repeated on three different chip samples, and the results are very consistent.

The antenna gain is calculated based on

$$G_{\mathrm{AUT}} = P_{\mathrm{AUT}} - P_{\mathrm{horn}} + G_{\mathrm{horn}} + \mathrm{Loss}_p \qquad (1)$$

in which all the terms given are in decibel scale: P_{AUT} and P_{horn} are the power received at the spectrum analyzer when using the AUT and a calibrated horn as receiving antennas, respectively. G_{horn} is the known gain of the calibrated horn antenna. Loss_p is the total insertion loss including the probe (1.6 dB), the shunt stub (0.4 dB), and the transition loss between probe tip and the on-chip CPW (0.5 dB), with a total loss of 2.5 dB. In Fig. 5, the measured broadside gain, indicated by dots, is obtained by averaging the measured data from three distinct gain measurements, and each frequency point has been averaged, including the nearest adjacent frequency points, to smooth out the interference effects described in Section II. Compared to the simulation curve, there is a 0–4-dB deviation (the maximum difference is at 100 GHz), which is acceptable for OCA measurements at 100 GHz [10].

As discussed in Section II, the accuracy of OCA gain measurements could be degraded by the interference between the

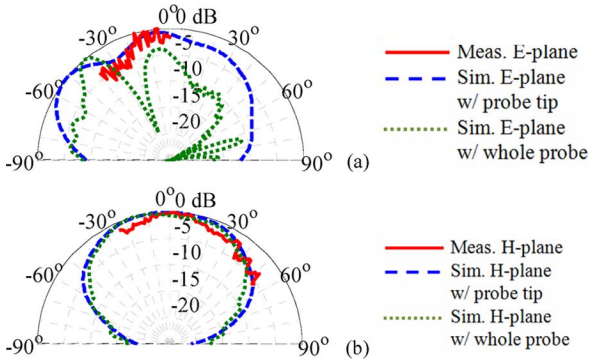

Fig. 6. Measured and simulated (a) E- and (b) H-plane normalized radiation patterns at 94 GHz.

probe, probing station, and AUT. For our case, since our antenna is put close to the chip edges, the edge field could be more sensitive to the chip surroundings. The interference due to the probe may occur in two ways.

1) The RF probe itself is acting as an antenna such that it receives/transmits power directly from/to the transmitting horn antenna. In [11], it was shown using simulations that a probe may radiate as a dipole at 60 GHz with -8 dBi gain. In our case, using the probe directly as a receiving (RX) antenna, we have measured a received power, radiated by the TX horn, 20 dB lower than the power received by the bowtie slot antenna. This means that we can neglect this interference in the present case.
2) The wave incident on the probe could be reflected (scattered) to the OCA, and vice versa, causing interferences. To alleviate this problem during radiation pattern measurements, very thin absorbers are used to surround the antenna, and also to partly cover the probe-head. It was observed that with careful placement of absorbers, the interference due to these reflections could be significantly reduced, and a smoother radiation pattern was obtained. Because of these issues, even though the simulation includes the probe, the results shown in Fig. 2 only estimate the degree of variation and still may not be fully capturing all the interferences in the measurement.

The normalized measured radiation pattern of the bowtie slot antenna at 94 GHz is shown in Fig. 6. The measured pattern is compared against the simulated cases, one with the probe-tip near the AUT [Fig. 2(a)] and one with the whole probe [Fig. 2(b)]. Due to the presence of certain obstacles in the probe station, the pattern measurement cannot be measured in the whole E- and H-planes. In the E-plane, the measurement could be done in only one quadrant, and the range is limited by 40° from the broadside direction. In the H-plane, the limit is 25° in one quadrant and 55° in the other quadrant of the upper hemisphere. The measured and simulated patterns from the case with probe tip are shown to have similar trends. Due to partial shielding effect from thin absorbers, the measured pattern does not show corrupted nulls in the E-plane as instead shown when the whole probe is included in simulation. The ripple of the radiation pattern is probably due to the interference between the probe and the AUT during measurement and shows the range of inaccuracy when measuring gain at *W*-band frequencies on a probe station. Interference can be constructive or destructive depending on the observation angle and is larger in the E-plane.

IV. Conclusion

We have shown a study of the performance of a fully integrated on-chip bowtie slot antenna operating at *W*-band frequencies. The antenna was placed on the topmost metal layer of a BiCMOS process with a ground below the silicon substrate. A measured wideband impedance bandwidth covering the whole *W*-band was obtained. Simulated and measured antenna input matching and radiation patterns are in good agreement. The measured broadside gain was 0–1 dBi with 2–4 dB uncertainty due to the interference caused by the probe during measurement, as discussed with a dedicated simulation analysis. The efficiency of this antenna solution is low, but gain measurements and simulations show some of the best performance published relative to fully integrated on-chip silicon-based antennas. While the use of hybrid antennas, which may consist of partially on-chip and off-chip solutions, is currently more efficient from a system link-budget perspective, fully on-chip antennas can provide a higher level of integration, thus resulting in cost benefits (at large volumes) in CMOS/SiGe-based fully integrated systems-on-chip. In addition to the advantages gained in system cost, size, and weight, these future on-chip-antennas are expected to have continually increasing electrical performance improvements at higher mm-wave frequencies.

Acknowledgment

The authors thank TowerJazz for antenna fabrication and ANSYS, Inc., for providing HFSS.

References

[1] H. M. Cheema and A. Shamim, "The last barrier: On-chip antennas," *IEEE Microw. Mag.*, vol. 14, no. 1, pp. 79–91, Jan.–Feb. 2013.
[2] Y. P. Zhang and D. X. Liu, "Antenna-on-chip and antenna-in-package solutions to highly integrated millimeter-wave devices for wireless communications," *IEEE Trans. Antennas Propag.*, vol. 57, no. 10, pp. 2830–2841, Oct. 2009.
[3] S. Beer, H. Gulan, C. Rusch, and T. Zwick, "Coplanar 122-GHz antenna array with air cavity reflector for integration in plastic packages," *IEEE Antennas Wireless Propag. Lett.*, vol. 11, pp. 160–163, 2012.
[4] U. R. Pfeiffer, J. Grzyb, L. Duixian, B. Gaucher, T. Beukema, B. A. Floyd, and S. K. Reynolds, "A chip-scale packaging technology for 60-GHz wireless chipsets," *IEEE Trans. Microw. Theory Tech.*, vol. 54, no. 8, pp. 3387–3397, Aug. 2006.
[5] S. Pan and F. Capolino, "Design of a CMOS on-chip slot antenna with extremely flat cavity at 140 GHz," *IEEE Antennas Wireless Propag. Lett.*, vol. 10, pp. 827–830, 2011.
[6] L. Gilreath, V. Jain, and P. Heydari, "A W-band LNA in 0.18-μm SiGe BiCMOS," in *Proc. IEEE ISCAS*, 2010, pp. 753–756.
[7] S. Beer and T. Zwick, "Probe based radiation pattern measurements for highly integrated millimeter-wave antennas," in *Proceedings 4th EuCAP*, 2010, pp. 1–5.
[8] S. A. Hosseini, F. Capolino, and F. De Flaviis, "A 44 GHz single-feed Fabry-Parot cavity antenna designed and fabricated on quartz," in *Proc. IEEE APSURSI*, 2011, pp. 1285–1288.
[9] H. Sanming, W. Lei, X. Yong-Zhong, L. T. Guan, Z. Bo, S. Jinglin, and Y. Xiaojun, "TSV technology for millimeter-wave and terahertz design and applications," *IEEE Trans. Compon., Packag., Manuf. Technol.*, vol. 1, no. 2, pp. 260–267, Feb. 2011.
[10] H. Debin, X. Yong-Zhong, G. Wang-Ling, H. Sanming, H. Wei, and M. Madihian, "130-GHz on-chip meander slot antennas with stacked dielectric resonators in standard CMOS technology," *IEEE Trans. Antennas Propag.*, vol. 60, no. 9, pp. 4102–4109, Sep. 2012.
[11] K. Mohammadpour-Aghdam, S. Brebels, A. Enayati, R. Faraji-Dana, G. A. Vandenbosch, and W. DeRaedt, "RF probe influence study in millimeter wave antenna pattern measurements," *Int. J. RF Microw. Comput.-Aided Eng.*, vol. 21, pp. 413–420, 2011.